RESEARCH ARTICLE

Mutual regulation between GDF11 and TET2 prevents senescence of mesenchymal stem cells

Jiaming Gao[1] | Hao Wang[1] | Junyan Shen[1] | Xiaojing Liu[2] | Xiaoqi Zhu[1] | Ce Huang[1] | Gongchen Li[3] | Yao Sun[3] | Zhongmin Liu[1,4] | Yi Eve Sun[1,2,3,5] | Hailiang Liu[1,4]

[1]Institute for Regenerative Medicine, Shanghai East Hospital, Tongji University School of Medicine, Shanghai, China

[2]Translational Center for Stem Cell Research, Tongji Hospital, Tongji University School of Medicine, Shanghai, China

[3]Department of Implantology, Shanghai Engineering Research Center of Tooth Restoration and Regeneration, School of Stomatology, Tongji University, Shanghai, China

[4]Shanghai Institute of Stem Cell Research and Clinical Translation, Shanghai East Hospital, Tongji University School of Medicine, Shanghai, China

[5]Department of Psychiatry and Biobehavioral Sciences, UCLA Medical School, Los Angeles, California, USA

Correspondence
Zhongmin Liu and Yi Eve Sun, Institute for Regenerative Medicine, Shanghai East Hospital, Tongji University School of Medicine, 200123, Shanghai, China.
Email: liu.zhongmin@tongji.edu.cn and yi.eve.sun@gmail.com

Hailiang Liu, Shanghai Institute of Stem Cell Research and Clinical Translation, Shanghai, China.
Email: hailiang_1111@tongji.edu.cn

Abstract
Growth differentiation factor 11 (GDF11) is a putative systemic rejuvenation factor. In this study, we characterized the mechanism by which GDF11 reversed aging of mesenchymal stem cells (MSCs). In culture, aged MSCs proliferate slower and are positive for senescence markers senescence-associated β-galactosidase and P16^{ink4a}. They have shortened telomeres, decreased GDF11 expression, and reduced osteogenic potential. GDF11 can block MSC aging in vitro and reverse age-dependent bone loss in vivo. The antiaging effect of GDF11 is via activation of the Smad2/3-PI3K-AKT-mTOR pathway. Unexpectedly, GDF11 also upregulated a DNA demethylase Tet2, which served as a key mediator for GDF11 to autoregulate itself via demethylation of the GDF11 promoter. Mutation of Tet2 facilitates MSC aging by blocking GDF11 expression. Mutagenesis of Tet2-regulated CpG sites also blocks GDF11 expression, leading to MSC aging. Together, a novel mutual regulatory relationship between GDF11 and an epigenetic factor Tet2 unveiled their antiaging roles.

KEYWORDS
cell senescence, mesenchymal stem cells, TET2

1 | INTRODUCTION

It has been recognized that aging involves epigenetic mechanisms. Old cells have very different epigenetic landscape as compared with young cells, which includes shortened telomeres, increased epigenetic markers (e.g., H4K20me3, γH2Ax) (Blasco, 2007; Lyu et al., 2018; Njajou et al., 2009; Siddiqui et al., 2015), and increased global DNA methylation levels (Hannum et al., 2013; Unnikrishnan et al., 2019). Ten-11 translocation methylcytosine dioxygenase (*Tet*) genes encode critical enzymes involved in active DNA demethylation (Wu & Zhang, 2017). It has been reported that reduced Tet2 expression is associated with aging of hippocampal adult neural stem cells (NSCs)

(Gontier et al., 2018; Li et al., 2017). In a heterochronic parabiosis rejuvenation model, Tet2 expression in hippocampus was restored and heightened Tet2 expression rejuvenated adult hippocampal NSC (Gontier et al., 2018). In contrast, knocking out of Tet2 in young hippocampi reduced neurogenesis and impaired learning (Li et al., 2017). Human genetic studies revealed increased frequency of somatic Tet2 mutations with age and Tet2 somatic mutations lead to increased risk for age-associated pathological conditions, such as cancer, cardiovascular diseases, and stroke (Burgess, 2015; Nadarajah et al., 2015).

A parabiosis related factor, growth differentiation factor 11 (GDF11) belongs to the transforming growth factor β super family. Whether GDF11 is the main rejuvenation factor in young blood that exerts antiaging effect in old animals during parabiosis or whether GDF11 has any antiaging effect, has been heavily debated (Egerman et al., 2015; Katsimpardi et al., 2014; Loffredo et al., 2013; Olson et al., 2015; Poggioli et al., 2016; Sinha et al., 2014; Smith et al., 2015; Walker et al., 2017). Our recent study using recombinant mature GDF11 (rGDF11) without bovine serum albumin (BSA) as a carrier, has confirmed results from Lee Rubin's group that tail vein injection of rGDF11 enhanced adult NSC activities and increased angiogenesis in old mouse brains (Katsimpardi et al., 2014). In addition, we have demonstrated that systemic application of rGDF11 can also enhance cognitive function of old animals (Liu, 2020). In that study, we showed that rGDF11 can increase cell proliferation, reduce expression of a cell senescence marker, P16^{ink4a}, lengthen telomere, and also positively autoregulate *GDF11* gene expression in NSCs by activation of the downstream Smad2/3-PI3K-AKT-mTOR pathway. Whether GDF11, via activation of the same pathway, exerts its antiaging function also in other types of stem cells has not been reported.

In the present study, we extended GDF11 research to mesenchymal stem cells (MSCs). MSCs can differentiate into bone, cartilage, and fat cells, and also have therapeutic values such as regulation of age-related autoimmunity. There are on-going clinical trials including using autologous MSC to treat osteo-arthritis, and various neural degenerative conditions. Unfortunately, when people age, their MSC also age, reducing therapeutic values of those cells. Being able to rejuvenate MSC, even in vitro, will allow for more effective MSC-based therapies with rejuvenated autologous cells. Aged MSC have shortened telomeres, proliferate slower, and reduce osteogenic potentials. They also have reduced expression of GDF11 messenger RNA (mRNA). Applying rGDF11 to cultured MSC reversed senescence phenotype and also elevated *GDF11* gene expression, forming a potential positive feedback loop. Similar to that in NSCs, rGDF11 also rejuvenated MSC and autoregulated itself via activation of the Smad2/3-PI3K-AKT-mTOR pathway. To our surprise, downstream of mammalian target of rapamycin (mTOR), rGDF11 also elevated Tet2 expression, which is mTOR dependent. Expectedly, Tet2 expression is reduced in aged MSC, whereas overexpression of Tet2 can rejuvenate MSC via increased expression of GDF11. Tet2, as a DNA demethylation agent, demethylated the GDF11 proximal promoter and activated transcription. Methylation of GDF11 proximal promoter appear to be age-dependent. Mutagenesis of Tet2, increased DNA methylation of GDF11 proximal promoter, reduced

GDF11 expression, and resulted in cell senescence. Moreover, mutagenesis of the GDF11 proximal promoter in MSC, also shutdown GDF11 transcription, caused cell senescence even though the cells still contain wild-type Tet2 alleles. Through this study, we revealed an epigenetic mechanism underlying GDF11-dependent rejuvenation of MSC, where a mutual regulatory relationship between GDF11 and Tet2 played a crucial antiaging role in MSC.

2 | MATERIALS AND METHODS

2.1 | Culture and characterization of human MSC (hMSC)

This study was approved by the Regional Committee for Medical Research Ethics of Tongji Hospital, Tongji University, School of Medicine. hMSC were isolated from human adipose tissue of patients undergoing fracture surgery without acute systemic disease, malignant tumors, or endocrine disorders. hMSCs were isolated and cultured according to previously described methods (Estes et al., 2010). hMSCs were validated by the expression of CD105, CD73, CD90, and CD44, and failure to express CD34, HLA-DR, CD45, CD14, and CD19. The multipotency of the hMSC was validated by differentiation into osteogenic, chondrogenic, and adipogenic lineages. hMSC were maintained in Dulbecco's modified Eagle medium/F-12 (Gibico) supplemented with 10% fetal bovine serum and non-essential amino acid (Gibico) at 37°C in a humidified atmosphere containing 5% CO_2.

2.2 | Adipogenic differentiation

Adipogenic differentiation ability was performed using the StemPro Adipogenesis Differentiation Kit (Gibico) according to manufacturer's instructions. After 14 days, the adipocyte phenotype (fat droplet formation) was evaluated by Oil Red o (Sigma) staining and nuclear were staining with 4′,6-diamidino-2-phenylindole (DAPI).

2.3 | Osteogenic differentiation

Osteogenic differentiation ability was performed using the StemPro Osteogenesis Differentiation Kit (Gibico) according to manufacturer's instructions. After 21 days, the osteoblast phenotype (calcium phosphate precipitates) was evaluated by Alizarin Red staining.

2.4 | Senescence-associated β-galactosidase (SA-β-gal) staining

hMSC, Tet2-mutant, Gdf11-mutant, and Control cells at different passages were seeded at 2×10^4 cells per well in the 24-well plates for 24 h before staining (triplicate for each group). SA-β-gal was

performed by using the Cell Senescence β-Galactosidase Staining Kit (Beyotime) according to the manufacturer's instructions. Cell nuclei were stained with DAPI at room temperature for 15 min. The senescent cells were stained blue under the microscope (Nikon ECLIPSE Ti) and percentage of positive cell with β-galactosidase to marked nuclei by DAPI was counted by ImageJ.

2.5 | Reactive oxygen species (ROS) measurement

Fluorometric Intracellular ROS Kit (Sigma) was used to measure the level of intracellular ROS according to manufacturer's instruction. hMSCs were cultured at 1×10^4 cells/well in 96-well plates for 24 h. Ten microliters of test compound solution was added to each well and then incubated at 5% CO_2, 37°C for 30 min. Following that, 100 µL/well Reaction Mix was added and further incubated at 5% CO_2, 37°C for 30 min. The fluorescence intensity (λex = 640/λem = 675 nm) were measured.

2.6 | Immunostaining

Cultured hMSC samples were treated with 4% paraformaldehyde for 10 min at room temperature. After three washes with phosphate-buffered saline (PBS), all slides were incubated in blocking buffer (5% BSA and 0.3% Triton X-100 in PBS) for 1 h at room temperature. Coverslips were immersed in primary antibody buffer (20 µL per coverslip) for incubation overnight at 4°C. The primary antibodies including anti-Ki67 (Abcam: #15580) was 1:500. The following day, the coverslips were washed three times with PBS. They were then incubated in buffers containing appropriate Alexa 488- or Alexa 568 secondary antibodies (Thermo Fisher Scientific) for 1 h at room temperature with 1:1000 dilution. DAPI staining was used to label nuclei for 15 min. Percentage of positive cells was calculated. At least three independent experiments for each condition were performed.

2.7 | Analysis of telomere lengths

Telomere lengths were measured as previously described (Cawthon, 2002). Briefly, each sample is amplified in two groups. The amplification of the telomere repeats is called T reaction and that of the *36B4* gene is called S reaction. The relative telomere relative ratio (T/S) = $2^{-\Delta\Delta Ct}$, ΔCT = CT(Telomere) – CT (36B4). Real-time polymerase chain reaction (PCR) were performed to measure telomere lengths and primer sequences were listed in Supporting Information: Table 1.

2.8 | Cell cycle analysis

Cell cycle analysis was performed using the Cell Cycle and Apoptosis Analysis Kit (Beyotime) according to manufacturer's instructions.

Briefly, cells were collected, washed with pre-cold PBS twice, and then fixed with 70% cold ethanol and stored at 4°C for 16 h. Cells were then resuspended in propidium iodide solution at 37°C in the dark for 30 min. All samples were washed and analyzed using Flow Cytometry (BD FACSVerse). All conditions were performed in triplicate.

2.9 | Cell apoptosis assay

The Annexin V-FITC Apoptosis Detection Kit (ab14085; Abcam) was used to evaluate levels of apoptosis of hMSC at different passages.

2.10 | Cell proliferation assay

Cell viability was evaluate using the Cell Counting Kit-8 (Dojindo Laboratories). hMSCs were placed in a 96-well plate at a density of 1×10^4 cells per well and treated with 10 µL Cell Counting Kit 8 (CCK8) reagent each well for 3 h at 37°C. The absorbance at 450 nm was measured by SpectraMax M5 Absorbance Reader.

2.11 | RNA extraction and quantitative real-time PCR analysis

Total RNA was isolated using Trizol reagent (Thermo Scientific). Contaminant DNA was eliminated by the addition of DNaseI (Ambion) followed by purification with phenol/chloroform. Ethanol, glycogen, and sodium acetate were used to achieve RNA precipitation. The quality and quantity of the extracted RNA were identified by Nanodrop 2000 (Thermo Scientific) and in 2100 Bioanalyser (Agilent). PrimeScript RT reagent Kit (Takara) was used to synthesize complementary DNA from 1 µg RNA. In addition, quantitative PCR (qPCR) was conducted by the Sybr-green super mix kit (Bio-Rad) and the Quantstudio 7 Flex Real-Time PCR system (Thermo Scientific). mRNAs were normalized to the level of reference gene *β-actin*. The $2^{-\Delta\Delta Ct}$ method was using to calculate gene expression and the primers sequences which used in the experiment were listed in Supporting Information: Table 1.

2.12 | RNA sequencing analysis

For RNA sequencing, RNA from cell samples were extracted by Trizol reagent (Invitrogen) according to manufacturer's instruction. After quality assessment of RNA by NanoDrop, Qubit3 (Invitrogen), and 2% agarose gel, 1000 ng high-quality RNA samples were used for sequencing library preparation. Sequencing libraries were constructed using NEBNext Ultra RNA Library Prep Kit from Illumina (NEB) according to manufacturer's recommendations. After quality assessment of the libraries by Agilent 2100 Bioanalyzer, samples were sequenced by HiSeq-2000 platform.

2.13 | Real-time measurement of glycolytic activities

Real-time monitoring of hMSC metabolic activities was performed using an XF96 Extracellular Flux Analyzer (Seahorse Bioscience), according to manufacturer's instructions (Faubert et al., 2014; Vincent et al., 2015). In brief, control and rGDF11-treated cells were plated at 5×10^3 per well in 96-well plates for 24 h before the assay. Cells were then incubated in a non-CO_2 incubator for 1 h at 37°C to allow for temperature and pH equilibration before loading into the XF96 apparatus. Cells were starved in glucose-free medium for 2 h, after which glucose was reintroduced (25 mM). Cells were then treated with 100 mM 2-DG (a glycolytic inhibitor). Real-time ECAR data in all the figures are representative of at least three independent biological experiments.

2.14 | Micro-computed tomography (μCT) analysis

For ex vivo μCT evaluations, a high-resolution tomography image system (μCT-50 Scano Medical AG) was used to measure trabecular bone parameters. Routine calibration was performed once a week using a three-point calibration phantom corresponding to a density range from air to cortical bone. All samples were scanned with voxel size of 10 μm, a 55 kVp X-ray potential, and a current of 109 μA. Briefly, 100 slices were scanned at the region of the distal femur beginning at the growth plate and extending proximally along the femur diaphysis. All trabecular bones from each selected slice were segmented for three-dimensional reconstruction to calculate the following parameters: bone volume to total volume ratio, trabecular number, trabecular separation, and trabecular thickness.

2.15 | Western blot analysis and antibodies

Cells were lysed in RIPA buffer (Beyotime Biotechnology, Catalog No. P0013B), containing protease inhibitor cocktail (Roche, Catalog No.04693159001), on the ice. The concentrations of protein were measured by BCA kit (Biomiga, Catalog No. PW0104). Protein samples were denatured with Loading Buffer (Beyotime Biotechnology, Catalog No. P0015L) for 5 min at 95°C. Twenty micrograms of samples per lane were loaded for sodium dodecyl-sulfate polyacrylamide gel electrophoresis and then transferred onto polyvinylidene difluoride membrane (Millipore, Catalog No. ISEQ. 00010). Following sealing with 5% skimmed milk, the membranes were incubated with primary antibodies overnight at 4°C. After incubated with horseradish peroxidase (HRP)-conjugated secondary antibodies, the immune-reactive protein bands were visualized by using Millipore's enhanced chemiluminescence (ECL, Catalog No. WBKLS0100) with the Amersham Imager 600 detection system (GE Healthcare Life Sciences). The western blot analysis results represent at least three independent biological experiments.

Antibodies information were listed as the following: Monoclonal mouse anti-β-Actin at 1:15,000 (Proteintech, 60008-1-1g), anti-α-tubulin at 1:10,000 (Sigma, T5168-.2ML); monoclonal rabbit anti-PI3K at 1:1000 (Abcam, ab151549), anti-S6K1 at 1:1000 (Abcam, ab32529), anti-AKT1 (phosphor S473) at 1:5000 (Abcam, ab81283), anti-SMAD2 at 1:5000 (Abcam, ab40855), anti-SMAD3 at 1:5000 (Abcam, ab40854), anti-mTOR at 1:5000 (Abcam, ab32028), anti-mTOR (phosphor S2448) at 1:10,000 (Abcam, ab109268), anti-SRC at 1:10,000 (Abcam, ab109381), anti-eNOS at 1:1000 (Abcam, ab199956); anti-AKT at 1:500 (Abcam, ab8805), anti-SMAD2 (phosphor S467) at 1:1000 (Abcam, ab53100), anti-SMAD3 (phosphor S423 + S425) at 1:2000 (Abcam, ab52903), anti-S6K1 (phosphor T389) at 1 μg/mL (Abcam, ab2571), anti-TET1 at 1:10,000 (Novus, nbp2-19290), anti-TET2 at 1:1000 (Proteintech, 21207-1-AP), anti-TET3 at 1:10,000 (Novus, nbp2-20602), anti-5-hmC at 0.2 μg/mL (Active Motif, 39791), and anti-GDF11 at 1:1000 (Abcam, ab124721).

2.16 | Chromatin immunoprecipitation (ChIP) assays

ChIP assays were conducted utilizing Magna ChIP™ HiSens Chromatin Immunoprecipitation Kit (Merck Millipore, Cat. No. 17-601) based on instructions provided by the manufacturer. The eluted pure DNA was used for PCR with primers matching human Gdf11 promoter segment (Supporting Information: Table 1). PCR program was designed below: The annealing temperatures for the first primer sets were 58°C, with 35 cycles. PCR results were revealed by electrophoresis on 2% agarose gel.

2.17 | Methylation assay

The methylation status of CpG sites within the GDF11 promoter was determined by bisulfite conversion using EZ DNA methylation-Gold kit (ZYMO Research, Catalog Nos: D5005). The CpG island of the GDF11 proximal promoter were predicted by http://www.urogene.org/cgi-bin/methprimer/methprimer.cgi (Li & Dahiya, 2002). CpG sites, divided into one pair of primers for amplification (Supporting Information: Table 1). The PCR program and analysis were performed by using the MethylTarget™ (Genesky Biotechnologies Inc.) according to the manufacturer's instructions.

2.18 | Lentiviral gene-editing systems

lentiCRISPR v2 from Addgene (Plasmid no. 52961, deposited by Feng Zhang) was used for Tet2 and Gdf11 promoter mutagenesis. Guide RNA targets were designed with the online software for F. Zhang's laboratory (http://crispr.mit.edu/) and inserted into the Crisp-Cas9 vector. The information of CRISP single guide RNA was shown in Supporting Information: Table 1. For Tet2 overexpression and control plasmids, we used pEZ-Lv201 purchased from Genecopoeia (EX-H3630-Lv201, EX-NEG-Lv201). Lentiviral plasmid 10 μg/dish and

package plasmids 6 µg/dish (δ8.9, VSVG) were cotransfected into HEK 293T cells using LentiFit (Hanbio, LET1000) for virus packaging by the manufacturer's instruction. The collected viral supernatant was concentrated by ultracentrifugation with 55,000g, 210 min (BECKMAN, XPN-80). Lentiviral infections were performed in hMSC as described by the Genecopoeia. Infected cells were selected by 1 µg/mL puromycin (Solarbio P8230-100mg) for 7 days.

2.19 | Luciferase activity assay

The Gdf11 promoter from −479 bp to +37 bp were synthesized and then constructed into pGL3-basic promoter vector (Promega). hMSC were cotransfected with PGL3-Gdf11-promoter plasmids and Renilla luciferase vector using Lipofectamine 2000 (Thermo Fisher, Catalog: 11668019) to perform luciferase reporter assays by the Dual-Luciferase Reporter Assay Kit (Promega, Catalog: E1910), 24 h after transfection. At least three independent experiments were performed for statistical analyses.

2.20 | Dot blotting

According to previous protocols, (Liu et al., 2016; Wu et al., 2018), the levels of cytosine modification were detected by dot blotting. DNA samples were diluted to 10 ng/µL in Tris-EDTA (TE) buffer with twofold dilutions, followed by addition of 1/4 volume 2 M NaOH–50 mM EDTA to each sample. DNA was denatured at 95°C for 10 min, then transferred quickly to ice, with addition of ice cold 2 M ammonium acetate according to 1:1 ratio for another 10 min. Meanwhile, incubation of the nitrocellulose membrane with dd-H_2O, then with 6× SSC buffer for 20 min was performed. After the membrane was rehydrated with TE buffer, loading of genomic DNA on to the membrane was performed, followed by washing with 2× SSC buffer, and cross-linked by UV light for 20 min. Following blocking with 5% skimmed milk, the membranes were incubated with primary antibodies overnight at 4°C. After incubation with HRP-conjugated secondary antibodies (Abcam, Catalog No. ab6789), the dots were visualized by using Millipore's ECL with the Amersham Imager 600 detection system (GE Healthcare Life Sciences).
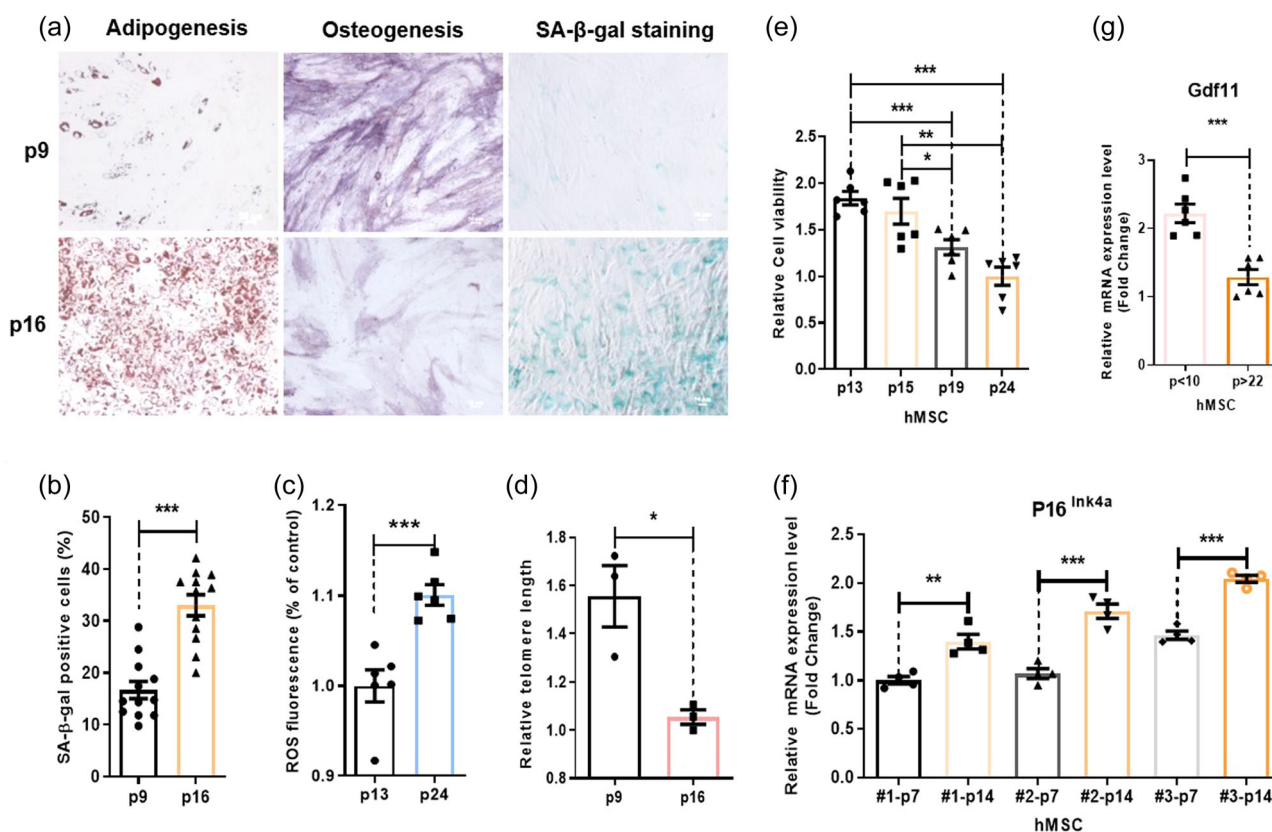

FIGURE 1 Senescence phenotypes of cultured human mesenchymal stem cell (hMSC). (a) Oil Red O staining, alkaline phosphatase staining, and senescence-associated β-galactosidase (SA-β-gal) staining of hMSC at an earlier passage (p9) and a later passage (p16). Scale bar, 50 µm. (b) SA-β-gal-positive cells increased in high number passaged hMSC cultures. (c) Mitochondrial reactive oxygen species (ROS) analysis of hMSC at an earlier passage (p13) and a later passage (p24). (d) Quantitative polymerase chain reaction (qPCR) detection of relative telomere length of hMSC at earlier passage (p9) and later passage (p16). (e) Cell viability assay to monitor cell senescence upon passaging. (f) quantitative real-time reverse-transcription PCR detection of a cell senescence marker P16Ink4a in hMSC at an earlier passage (p7) and a later passage (p14). (g) Growth differentiation factor 11 (GDF11) messenger RNA (mRNA) decreased in high number-passaged hMSC cultures. Data are shown as mean ± SEM; statistical analysis was performed with t test in (B–G); *p < 0.05, **p < 0.01, ***p < 0.001.

3 | RESULTS

3.1 | Aging features of MSC

To study MSC aging, we first characterized properties of aged human MSC in culture. We found long-term passaging can cause cell senescence of hMSC. Old hMSC have reduced osteogenic and increased adipogenic potentials (Figure 1a). Old hMSC contained more SA-β-gal (cell senescence maker) signals, increased levels of ROS, and shortened telomere (Figure 1b–d and Supporting Information: Figure S1). Cell viability assessment using the CCK8 assay indicated that cultures with high-number passages have reduced total viable cells, which could be due to decreased cell proliferation or increased cell death, or both. Our
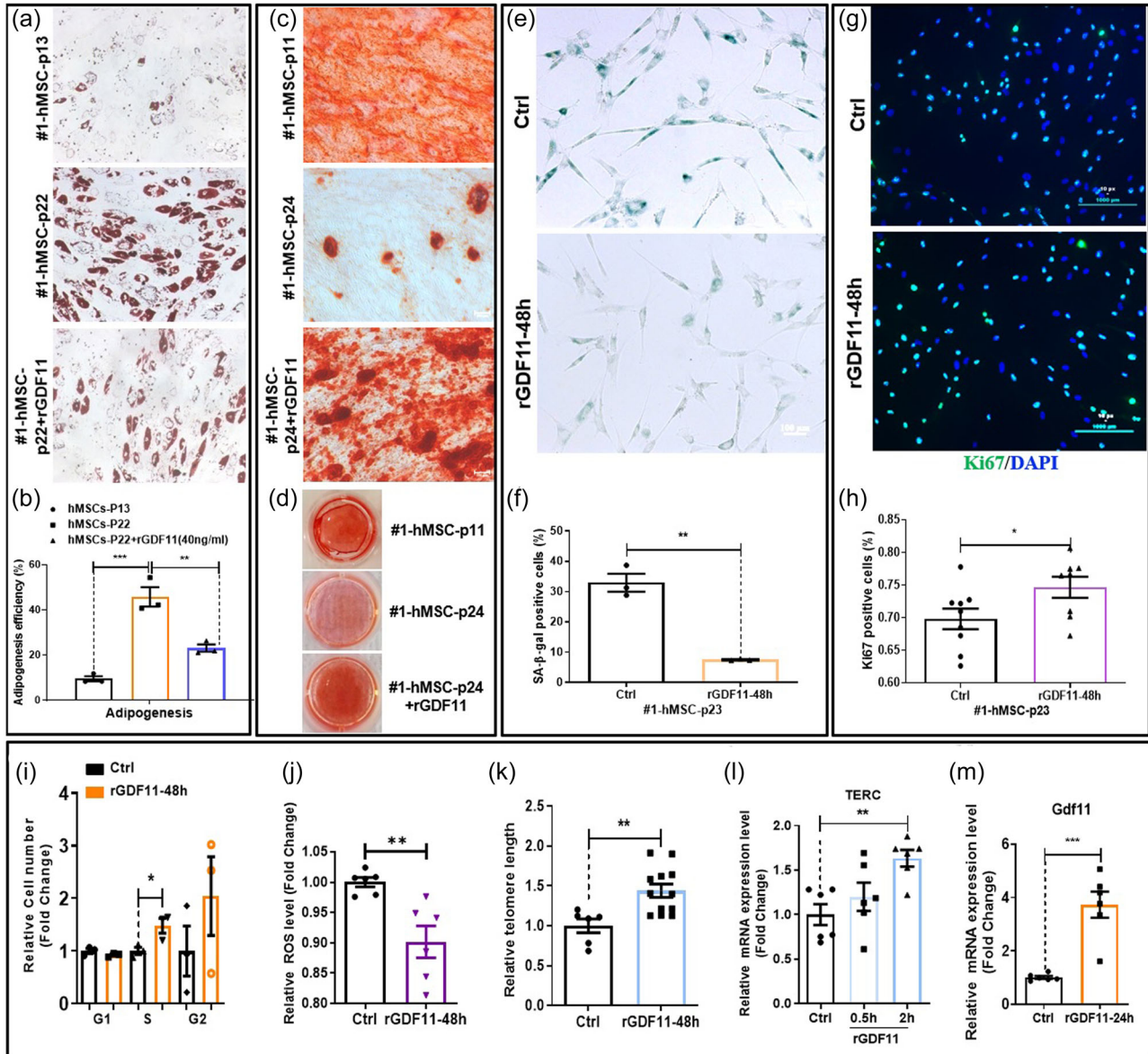

FIGURE 2 Influences of growth differentiation factor 11 (GDF11) on replicative senescence of human mesenchymal stem cell (hMSC). (a, b) Oil Red O staining to measure adipogenic ability of hMSC at an earlier passage (p13), a later passage (p22), and a later passage (p22) treated with GDF11 (40 ng/mL). Scale bar, 100 μm. (c, d) Alizarin Red S staining to determine osteogenic potential of hMSC at an earlier passage (P11), a later passage (p24), and a later passage (p24) treated with GDF11 (40 ng/mL). Scale bar, 100 μm. (e, f) Senescence-associated β-galactosidase (SA-β-gal) staining of hMSC treated with GDF11 (40 ng/mL) for 48 h at a late passage (p23). Scale bar, 100 μm. (g, h) Immunofluorescence staining and quantification of Ki67 in hMSC treated with GDF11 (40 ng/mL) for 48 h at a later passage (p23). Scale bar, 1000 μm. (i) Cell cycle phase distributions of hMSC treated with GDF11 (40 ng/mL) for 48 h at passage (p23) were determined using flow cytometry. (j) Mitochondrial reactive oxygen species (ROS) in hMSC with or without GDF11 treatment for 48 h at passage 24 (p24). (k) Quantitative polymerase chain reaction (qPCR) detection of relative telomere lengths of hMSC treated with GDF11 (40 ng/mL) for 48 h at passage 23 (p23). (l, m) Quantitative real-time reverse-transcription PCR detection of a telomerase RNA component (TERC) and GDF11 expression. Data are shown as mean ± SEM; statistical analysis was performed with t test in (b, f, h–m); $^*p < 0.05$, $^{**}p < 0.01$, $^{***}p < 0.001$.

further study indicated that there were no differences in degrees of cell-death between low- and high-number-passaged cells (Supporting Information: Figure S2). These two combined assays suggest that old-hMSC have reduced cell proliferation capacity (Figure 1e). As expected, higher-number-passaged cells express higher levels of another cell senescence marker, P16^{ink4a} (Figure 1f). Similar to aged NSCs, old hMSC also express reduced levels of GDF11 mRNA (Figure 1g). These features are consistent from different lines of hMSC (Figure 1f and Supporting Information: Figure S1).

3.2 | GDF11 reverses aging of hMSC and enhances osteogenesis in vivo

Similar to NSCs, when rGDF11 at a dose of 40 ng/mL was added to high-number-passaged hMSC cultures, overall rejuvenation of hMSC can be observed. hMSC regain osteogenic, reduced adipogenic, potentials (Figure 2a–d), decreased SA-β-gal signals (Figure 2e,f), and increased proliferation (Figure 2g,h). Cell cycle analyses indicated that GDF11-treated hMSC cultures have more cells in S and G2 phases and less cells in G1 phase (Figure 2i). rGDF11 treatment reduced ROS
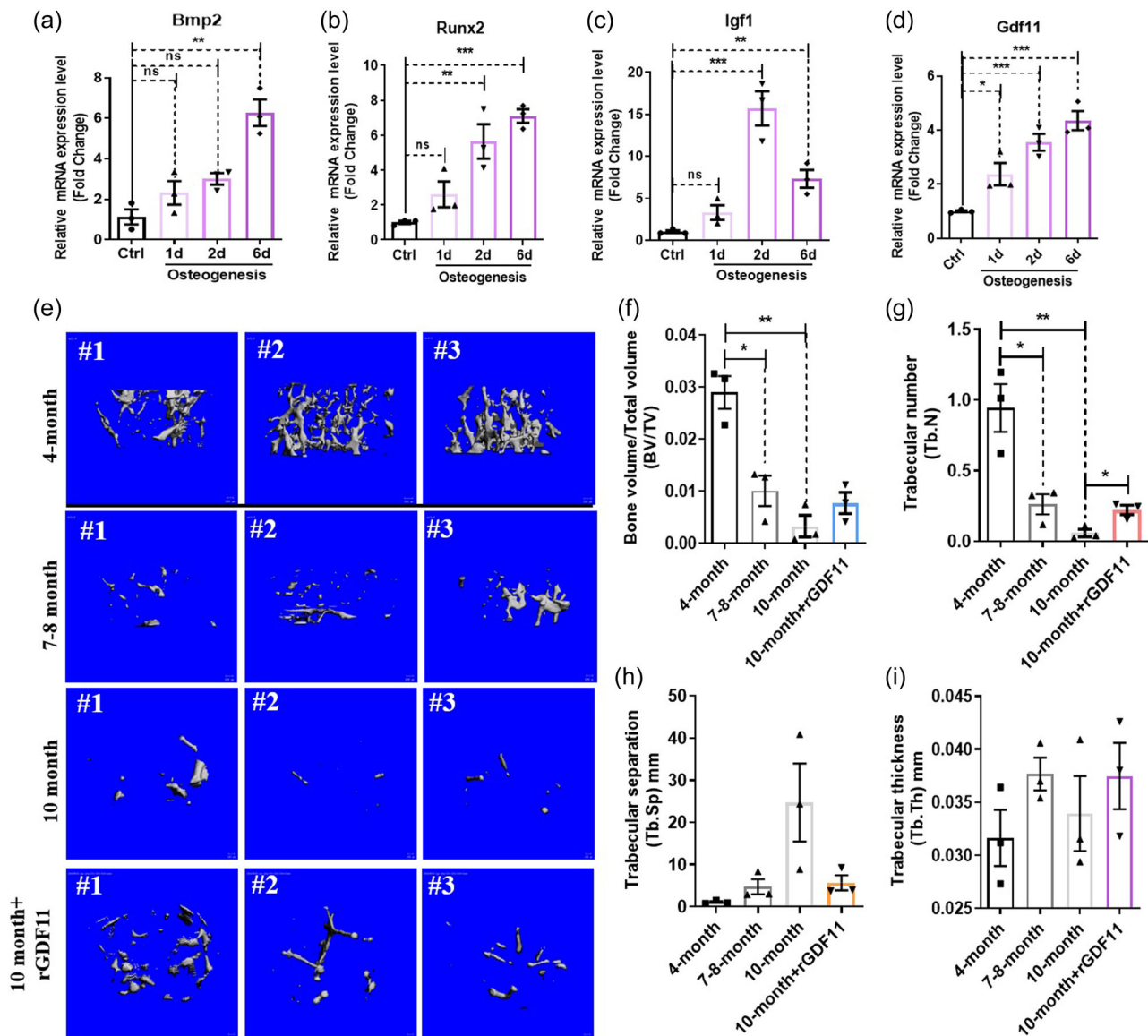

FIGURE 3 Effects of recombinant mature growth differentiation factor 11 (rGDF11) on osteogenic differentiation in vitro and in vivo. (A–D) Quantitative real-time reverse-transcription polymerase chain reaction (qRT-PCR) analysis of Bmp2, Runx2, Igf1, and Gdf11 expression in human mesenchymal stem cell (hMSC) during osteoblast differentiation at 1, 2, and 6 days upon differentiation. (e–i) Representative micro-computed tomography (μCT) images of femoral trabecular. (e) Scale bars, 100 μm. Quantitative μCT analysis of BV/TV (f), Tb.N (g), and Tb.Th (i) showed suppression of bone loss in 10 months + rGDF11 group. $n = 3$ per group. Quantitative μCT analysis of Tb.Sp (h) showed decreased femoral trabecular spacing in 10 months + rGDF11 group. $n = 3$ per group. BV/TV, bone volume/tissue volume ratio; Tb.N, trabecular number; Tb.Th, trabecular thickness; Tb.Sp, trabecular separation. Data are shown as mean ± SEM; statistical analysis was performed with t test in (a–d and f–i); *$p < 0.05$, **$p < 0.01$, ***$p < 0.001$. "ns" no difference.

levels in aged hMSC (Figure 2j). rGDF11-treated hMSC also have lengthened telomeres and have elevated expression of TERC, HNRNP2AB1, and HNRNPD, components of the telomerase complex (Figure 2k,i and Supporting Information: Figure S3A–C). In hMSC, rGDF11 positively autoregulated GDF11 gene expression (Figure 2m). Unbiased transcriptomic analyses of young and old hMSC cultures and old hMSC treated with rGDF11 at different time points, revealed a gene cluster (the pink module), which expressed at higher levels in young hMSC and increased expression by rGDF11 treatment at all time points examined (Supporting Information: Figure S3D–F). Gene Ontology analysis revealed enrichment of genes involved in cell cycle and glycolysis in this module. We subsequently determined whether rGDF11 indeed enhanced glycolysis using the "Seahorse metabolic testing device" (Supporting Information: Figure S3G–I). Results confirmed enhancement of glycolysis in hMSC by rGDF11 treatment. Metformin was used as a positive control in these assays.

When hMSC were drove for osteogenesis, bone differentiation-related genes Bmp2, Runx2, Igf1 increased expression. GDF11 interestingly also increased expression during osteogenesis (Figure 3a–d). It is well known that aged bone marrow is called "yellow" marrow, indicative of increased adipogenesis. Aged bone marrow also has reduced osteogenic potentials. To determine whether GDF11 may promote osteogenesis from MSC in vivo, in aged animals, we analyzed bone structures using μCT in aged animals treated with rGDF11 via the tail vein. Data indicated that GDF11 can partially reverse age-dependent bone loss (Figure 3e–i). Interestingly, the aforementioned osteogenesis-related factors GDF11, Bmp2, Runx2, and Igf1 all decreased expression, even in aged human blood samples, correlating well with age-related decline in osteogenesis (Supporting Information: Figure S4A,B,D,E,G,H). However, unlike GDF11, the expression of these other three osteogenesis-related genes in human blood samples have no correlations with cognitive function (Supporting Information:
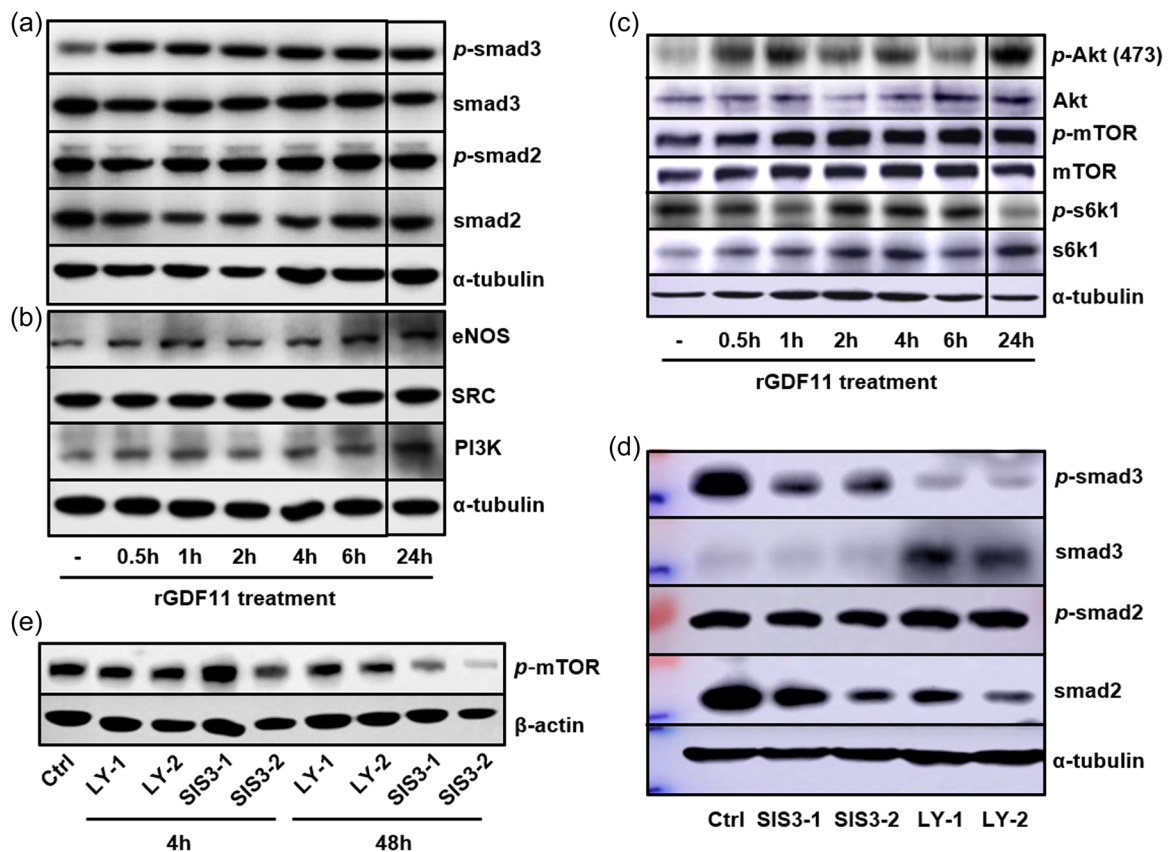

FIGURE 4 Recombinant mature growth differentiation factor 11 (rGDF11) mediates its antiaging function by activating the SMAD2/3-PI3K-AKT-mTOR pathway. (a) Representative western blot analysis of phosphor or total protein for smad2 or smad3 in human mesenchymal stem cell (hMSC) treated with rGDF11 (40 ng/mL) for 0.5, 1, 2, 4, 6, and 24 h. (b) Representative western blot analysis of total protein for eNOS, SRC, or PI3K in hMSC treated with rGDF11 (40 ng/mL) for 0.5, 1, 2, 4, 6, and 24 h. (c) Representative western blot analysis of phosphor or total protein for Akt, mTOR, and s6k1 in hMSC treated with rGDF11 (40 ng/mL) for 0.5, 1, 2, 4, 6, and 24 h. (d) Representative western blot analysis of phosphor or total protein for SMAD2 or SMAD3 in hMSC treated with the inhibitor of SMAD2 or SMAD3, LY2109761, or SIS3, respectively, for 24 h. (e) Representative western blot analysis of phosphor protein for mTOR in hMSC (p9) treated with inhibitor of SMAD2 or SMAD3, LY2109761, or SIS3, respectively, for 4 and 48 h. All western blot analyses were done from at least three independent experiments, and results were consistent. mTOR, mammalian target of rapamycin; PI3K, phosphatidylinositol 3-kinase.

Figure S4C,F,I), suggesting that GDF11 will not only promote the osteogenesis of MSCs, but also will affect the brain function by regulating other cells.

3.3 | GDF11 rejuvenates hMSC via SMAD2/3-PI3K-AKT-mTOR signaling pathway

Similar to NSCs, hMSC when stimulated with rGDF11 also activated Smad2/3 phosphorylation and downstream PI3K-AKT and mTOR signaling events (Figure 4a–c). Both Smad2 and Smad3 inhibitors blocked GDF11-induced mTOR phosphorylation/activation (Figure 4d,e), and inhibition of PI3K/mTOR blocked GDF11-enhanced osteogenesis from hMSC (Figure 5a). In addition, GDF11-caused reduction of $P16^{ink4a}$ could be reversed and further increased by rapamycin and BEZ235 (Figure 5b). Furthermore, Aging-related telomere shortening of hMSC could also be reversed by rGDF11 treatment, and such GDF11 function can be

blocked by the PI3K/mTOR inhibitor, BEZ235 (Figure 5c). Taken together, GDF11 activated intracellular Smad2/3-PI3K-AKT-mTOR pathway to achieve cell rejuvenation of MSC, similar to NSCs (Figure 5d).

3.4 | Tet2 is a rejuvenation factor activated by rGDF11 via a PI3K-mTOR and also induces *GDF11* gene expression

As a DNA demethylase, TET2 also plays an important role in the aging of the body. The relationship between TET2 and GDF11 was also validated in our results of subsequent experiments. In hMSC GDF11 treatment also elevated expression of an active DNA demethylase Tet2 in a PI3K-mTOR dependent manner (Figure 6a). Among the three Tet genes, *Tet1*, *2*, and *3*, only *Tet2* is highly expressed in hMSC (Supporting Information: Figure S5A,B). Interestingly, similar to GDF11, Tet2 expression also declined in aged hMSC
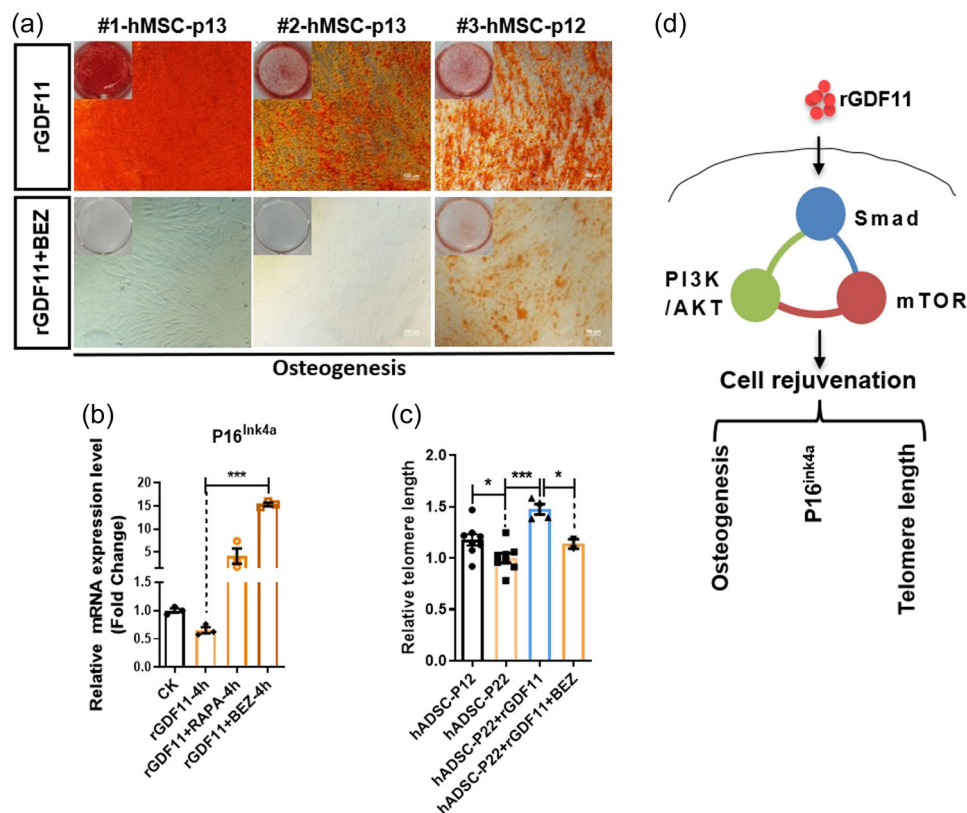

FIGURE 5 Growth differentiation factor 11 (GDF11) rejuvenated human mesenchymal stem cell (hMSC) through Smad2/3-PI3K-mTOR. (a) During the osteogenic induction, hMSC were treated with GDF11 (40 ng/mL) or cotreated with BEZ (inhibitor of PI3K and mTOR signaling) (25 nM). Calcium deposition was determined by Alizarin Red S staining, indicative of osteogenesis. Scale bar, 100 μm. (b) hMSCs were treated with GDF11 (40 ng/mL) or cotreated with BEZ or RAPA (inhibitor of mTOR signaling) (100 nM) for 4 h. Messenger RNA (mRNA) levels of P16ink4a were measured by quantitative real-time reverse-transcription polymerase chain reaction (qRT-PCR). (c) Relative telomere length of hMSC treated with GDF11 (40 ng/mL) or cotreated with BEZ (25 nM). (d) Summary of our results including those in the Figure S8B. GDF11 rejuvenates hMSC through the Smad-PI3K-mTOR pathway and modulates the activity of osteogenic differentiation, P16ink4a and telomere length. Data are shown as mean ± SEM; statistical analysis was performed with t test in (b and c); *$p < 0.05$, ***$p < 0.001$. mTOR, mammalian target of rapamycin; PI3K, phosphatidylinositol 3-kinase.
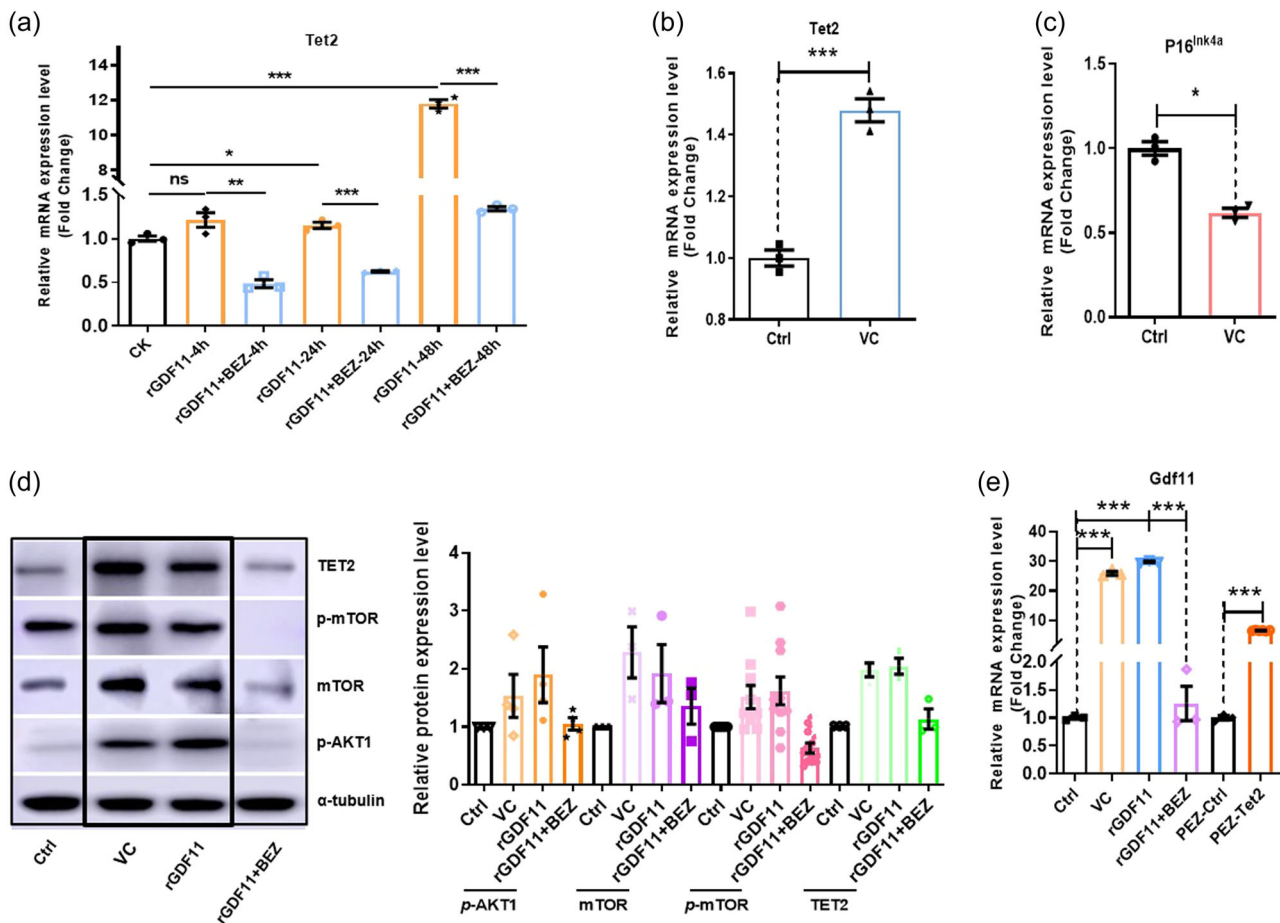
FIGURE 6 Tet2 expression is elevated by growth differentiation factor 11 (GDF11) via a PI3K-mTOR and also induces GDF11. (a) Tet2 expression level in human mesenchymal stem cell (hMSC) treated with recombinant mature GDF11 (rGDF11) (40 ng/mL) or both of BEZ (25 nM) and rGDF11 (40 ng/mL) for 4, 24, and 48 h by quantitative real-time reverse-transcription polymerase chain reaction (qRT-PCR) analysis. (b) Tet2 expression level in hMSC treated with vitamin C (VC, 50 ng/mL) for 48 h by qRT-PCR analysis. (c) P16ink4a expression levels in hMSC treated with or without VC for 48 h by quantitative PCR (qPCR) analysis. (d) p-AKT1, p-mTOR, mTOR, and Tet2 protein levels detected by western blot analysis in hMSC with different treatments. hMSC treated with VC (50 ng/mL), rGDF11 (40 ng/mL), and both of BEZ (25 nM) and rGDF11 (40 ng/mL) for 48 h. (e) qRT-PCR analysis for Gdf11 expression level in hMSC treated with VC (50 ng/mL), rGDF11 (40 ng/mL), and both of BEZ (25 nM) and rGDF11 (40 ng/mL) for 48 h, and either infected with a control virus or with a tet2 overexpression viral vector. Data are shown as mean ± SEM; statistical analysis was performed with t test or posthoc t test; $^*p < 0.05$, $^{**}p < 0.01$, $^{***}p < 0.001$. "ns" no difference. mTOR, mammalian target of rapamycin.

(Supporting Information: Figure S5C-F). Also, similar to GDF11, in human blood samples Tet2 expression declined with age and is positively correlated with cognitive functions (Supporting Information: Figure S5G–I). As vitamin C (VC) has been shown to activate Tet enzymes (Blaschke et al., 2013; Chen et al., 2013; Young et al., 2015), we used VC to increase Tet2 activities and found that VC treatment increased Tet2 and decreased senescence marker P16ink4a mRNA levels (Figure 6b,c). Moreover, VC, similar to GDF11, appeared to activate the Smad2/3-PI3K-AKT-mTOR pathway (Figure 6d). Again, similar to GDF11, VC also elevated GDF11 gene expression (Figure 6e). To determine whether the effect of VC on GDF11 upregulation is, at least in part, via Tet2, we overexpressed Tet2 in hMSC, and found that Tet2 overexpression increased GDF11 mRNA (Figure 6e), indicative of a "GDF11-Tet2-GDF11 gene expression" autoregulatory loop.

3.5 | Tet2 increased GDF11 gene expression by demethylation of the GDF11 promoter, and GDF11 can also regulate Tet2 gene expression

To confirm that Tet2 positively regulates GDF11 gene expression, we mutagenized Tet2 in hMSC using the Crispr-Cas9 gene-editing technology (Supporting Information: Figure S6). As shown in Figure 7a,b, Tet2-mutant hMSC has significantly reduced Tet2 and GDF11 expression. Consequently, Tet2 deficient hMSC appeared to facilitate senescence process by reducing osteogenic potentials, increasing SA-β-gal+ cells and increasing P16ink4a expression (Figure 7c–f). Together, these data demonstrated important roles of Tet2 in regulation of hMSC aging. To further determine the molecular mechanism by which Tet2 positively regulated GDF11 gene expression, we performed ChIP-PCR assay, and demonstrated that TET2
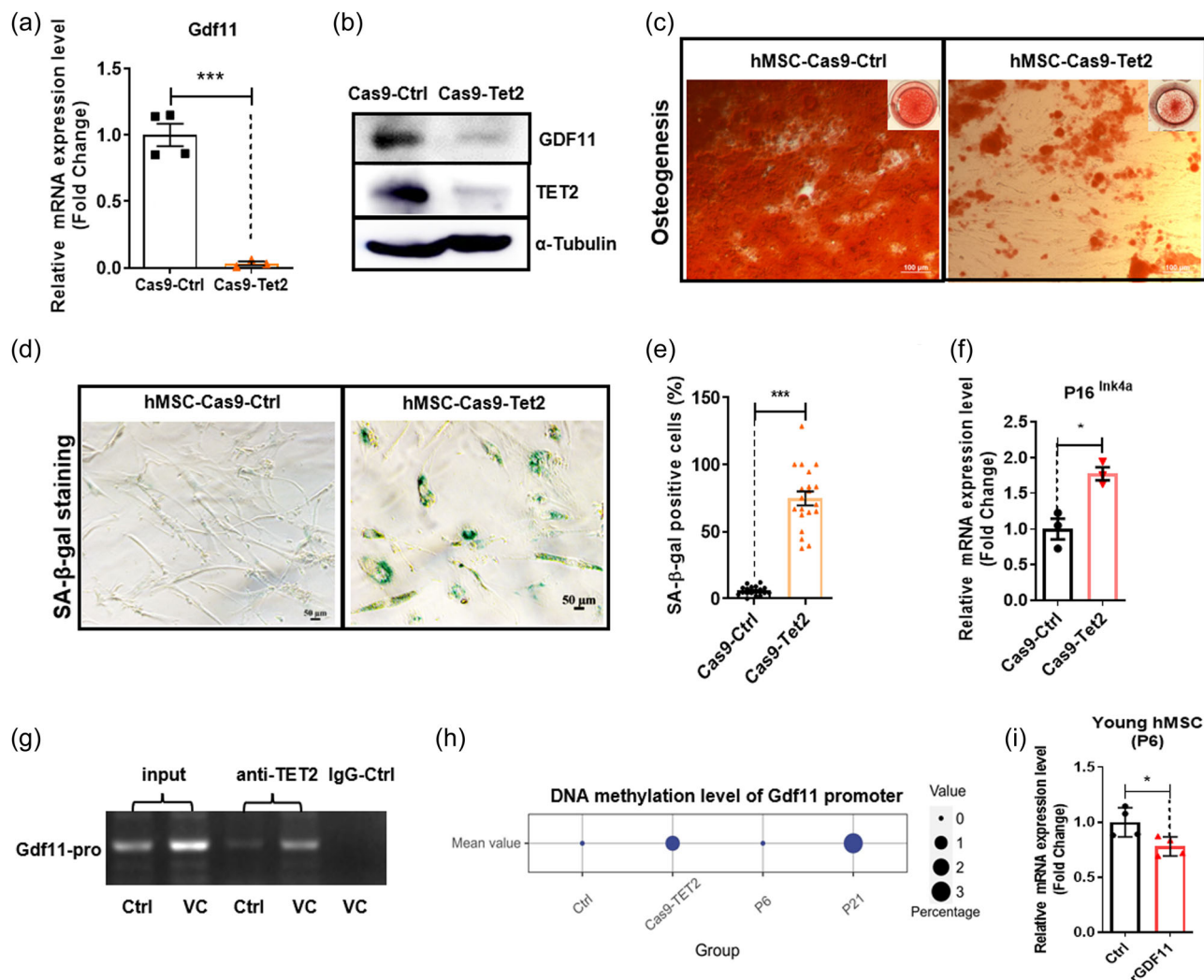
FIGURE 7 Mutagenesis of Tet2-blocked growth differentiation factor 11 (GDF11) expression, leading to mesenchymal stem cell (MSC) senescence. (a) Gdf11 expression level in hMSC Tet2 mutant (Cas9-Tet2) and Cas9-control cultures by quantitative real-time reverse-transcription polymerase chain reaction (qRT-PCR) analysis. (b) Tet2 protein level by western blot analysis in Cas9-Tet2 and Cas9-control. (c) Osteoblast differentiation identified by alizarin red staining in hMSC in Cas9-control and Tet2 mutant. (d) Senescence-associated β-galactosidase (SA-β-gal) staining of hMSC in Cas9-control and Tet2 mutant. (e) Percentage of SA-β-gal-positive cells increased in Cas9-Tet2 cultures. (f) P16Ink4a expression level in Cas9-Tet2 and Cas9-control cultures by qRT-PCR analysis. (g) Chromatin immunoprecipitation (ChIP)-qPCR Assay showing Tet2 binding to the GDF11 promoter region (−670 to −480 bp) in hMSC treated with or without VC (50 ng/mL) for 72 h. (h) Gdf11 promoter DNA methylation level by bisulfite sequencing analysis in Cas9-Tet2 and Cas9-control, hMSC at passage 6, and hMSC at passage 23. (i) qRT-PCR analysis for Gdf11 expression level in Young-hMSC (P6) treated with recombinant mature GDF11 (rGDF11) (40 ng/mL) for 48 h. Data are shown as mean ± SEM; statistical analysis was performed with t test in (a, e, f, i); *$p < 0.05$, ***$p < 0.001$.

protein was associated with the GDF11 promoter (Figure 7g). We further used bisulfite sequencing to determine whether there was any CpG methylation/demethylation event proximal to the transcription start site that was regulated by Tet2. The results showed that Tet2 deficient hMSC indeed led to increased DNA methylation level of GDF11 proximal promoter. As expected, higher-number-passaged hMSC also have higher DNA methylation level of GDF11 proximal promoter than low-number-passaged hMSC (Figure 7h). Using luciferase assay we showed that this promoter region (−479bp to +37 bp) contained age-dependent regulatory element(s) as well as Tet2-dependent regulatory element(s), because the luciferase activity

was reduced when tet2 was mutated (Supporting Information: Figure S7). Interestingly, in young hMSC, where the promoter of GDF11 were hypomethylated, treatment of rGDF11 failed to induce GDF11 mRNA expression (Figure 7i), suggesting that the GDF11-Tet2-GDF11 autoregulatory loop was only functional in aged hMSC with methylated GDF11 promoter.

To further determine whether GDF11 can regulate Tet2 gene expression, we again performed gene editing to mutagenize GDF11 proximal promoter. The resulting GDF11 promoter mutation showed deletion of some sequences (Figure 8a), thus hMSC carrying mutant GDF11 promoter, like Tet2-deficient hMSC, have significantly
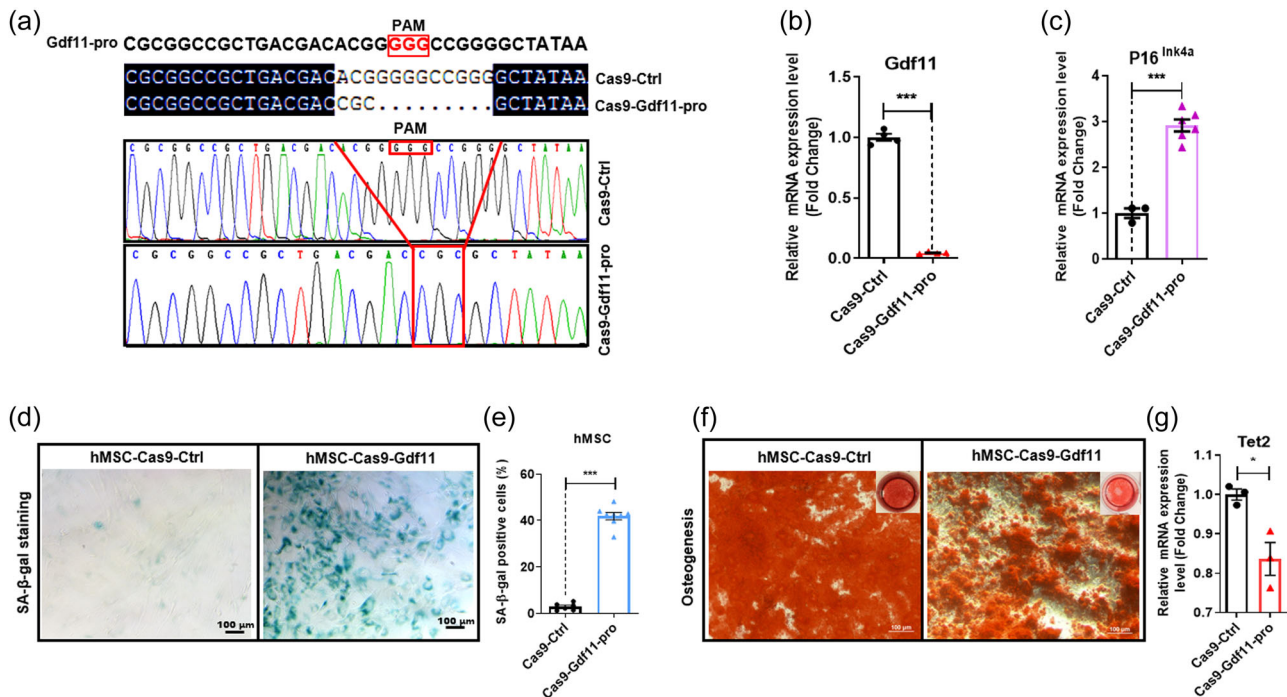
FIGURE 8 Growth differentiation factor 11 (GDF11) was also a rejuvenation factor can regulate Tet2 gene expression. (a) Using CRISPR/Cas9 system to mutagenize Gdf11 promoter targeting CpG sites. DNA sequencing analysis of Gdf11 promoter deletion after CRISPR/Cas9-mediated-mutagenesis in human mesenchymal stem cell (hMSC). (b) Gdf11 expression in Cas9-control and GDF11 promoter mutant hMSC. (c) P16ink4a expression level in Gdf11 mutant group and Cas9-control cultures by quantitative real-time reverse-transcription polymerase chain reaction (qRT-PCR) analysis. (d) Senescence-associated β-galactosidase (SA-β-gal) staining of hMSC in Cas9-control and Gdf11 mutant group. (e) Percentage of SA-β-gal-positive cells increased in Gdf11 mutant group. (f) Osteoblast differentiation identified by alizarin red staining in hMSC in Cas9-control and Gdf11 mutant group. (g) Tet2 expression in Cas9-control and GDF11 promoter mutant hMSC. Data are shown as mean ± SEM; statistical analysis was performed with t test in (b, c, e, g); $*p < 0.05$, $**p < 0.01$, $***p < 0.001$.

reduced *GDF11* gene expression (Figure 8b), and also elevated senescence markers P16^{ink4a} and SA-β-gal signals (Figure 8c–e), as well as reducing osteogenic potentials (Figure 8f), indicative of facilitated aging. In GDF11 promoter mutant cells, Tet2 mRNA levels remained relatively high, even though a statistically significant slight decrease of Tet2 mRNA levels was observed (Figure 8g). This indicated that Tet2, although could be regulated by GDF11, was also under the control of other factors.

Theoretically Tet2 should have broad targets, not just GDF11, one would expect that Tet2 mutation should give more severe phenotype than GDF11 promoter mutation, because GDF11 promoter mutations should only directly influence expression of one gene, that is, *GDF11*. The observation, however, indicated that GDF11 promoter mutation led to very strong aging phenotype, suggesting that GDF11 was perhaps one of the most important targets of Tet2, which negatively regulated hMSC aging. Consistently, in human blood samples, when we plotted GDF11 mRNA levels and promoter methylation levels along with age, we found that especially between the 30–40- and 60–80-year-old range, extremely significant correlations of these two parameters with aging were apparent (Supporting Information: Figure S8A), further suggesting the importance of DNA methylation-related epigenetic regulation of GDF11 expression during aging progression. A working model of mutual

regulation between GDF11 and Tet2 was presented in Supporting Information: Figure S8B.

4 | DISCUSSION

Through this study we revealed, for the first time, an epigenetic mechanism by which GDF11 rejuvenated hMSC, via the activation of a DNA demethylation enzyme, Tet2. Tet2 also appeared to be a rejuvenation factor. Surprisingly, the underlying mechanisms by which Tet2 rejuvenated hMSC was through demethylation of specific CpG sites within the GDF11 promoter and activated GDF11 gene transcription. Presumably, a positive feedback loop, GDF11 to PI3K-mTOR, to Tet2 to GDF11, may be a core antiaging pathway, and GDF11 is a key rejuvenation factor, even though recently many studies challenged this conclusion (Egerman et al., 2015; Smith et al., 2015). This study, together with our NSC study indicated very similar actions and signaling pathways by which GDF11 rejuvenated two types of stem cells, hMSC and NSCs. Given that Tet2 has recently been reported to be antiaging of adult mouse hippocampal NSCs, we predict that in NSCs, this GDF11-PI3K/mTOR-Tet2-GDF11 regulatory loop also exists. In addition, it appears that human peripheral blood mononucleated cells have similar age-related

alterations of GDF11 and Tet2 expression, as well as GDF11 promoter methylation properties, we predict that what we discovered here may apply to more cell types including immune cells. It remains to be determined whether muscle cells are regulated differently or whether details in the experimental procedure (such as whether or not BSA was used) caused discrepancy in experimental observations.

From this study, GDF11, in addition to having antiaging function in hMSCs, may also directly promote osteogenesis. Whether GDF11 regulates these two related biological processes via the same mechanism remained to be determined. A key experiment would be to test whether Tet2 is involved in osteogenesis. Moreover, how mTOR activation leads to Tet2 activation is a very important question, which shall be addressed in the near future. Taken together, it is becoming clear that GDF11 is definitely a rejuvenation factor for at least a good collection of different types of stem cells and perhaps immune cells and other cell types in the body. Moreover, the GDF11-PI3K/mTOR-Tet2-GDF11 positive regulatory loop could be a core antiaging mechanism and a good pathway for drug target. Any interventions that can intersect this loop, for example, VC to activate Tet2, may activate the whole loop and achieve antiaging effect. Given that GDF11 can be regulated at multiple posttranscriptional steps, for example, protein translation, proteolysis, secretion, and so on, this positive regulatory loop is likely subjected to various inhibitory regulations during aging. Lastly, perhaps not only GDF11 itself but also GDF11-rejuvenated MSC may be used as antiaging treatments for whole organisms.

5 | CONCLUSIONS

In summary, our present study shows that GDF11 is a rejuvenation factor. GDF11 can block MSC aging in vitro and reverse age-dependent bone loss in vivo. The antiaging effect of GDF11 is via activation of the Smad2/3-PI3K-AKT-mTOR pathway. GDF11 also upregulated a DNA demethylase Tet2, which served as a key mediator for GDF11 to autoregulate itself via demethylation of the GDF11 promoter. Such a finding revealed a novel mutual regulatory relationship between GDF11 and Tet2, and an epigenetic mechanism underlying the antiaging function of GDF11.

AUTHOR CONTRIBUTIONS

Jiaming Gao, Hao Wang, Junyan Shen, Xiaojing Liu, Xiaoqi Zhu and Ce Huang performed experiments. Hailiang Liu analyzed data. Gongchen Li and Yao Sun developed and provided micro-computed tomography (μCT) analysis. Hailiang Liu, Zhongmin Liu, and Yi Eve Sun supervised the project. Hailiang Liu and Yi Eve Sun designed the project and wrote the paper.

CONFLICT OF INTEREST STATEMENT

The authors declare no conflict of interest.

ORCID

Hailiang Liu https://orcid.org/0000-0002-5521-3746

REFERENCES

Blaschke, K., Ebata, K. T., Karimi, M. M., Zepeda-Martínez, J. A., Goyal, P., Mahapatra, S., Tam, A., Laird, D. J., Hirst, M., Rao, A., Lorincz, M. C., & Ramalho-Santos, M. (2013). Vitamin C induces Tet-dependent DNA demethylation and a blastocyst-like state in ES cells. *Nature*, *500*, 222–226.

Blasco, M. A. (2007). The epigenetic regulation of mammalian telomeres. *Nature Reviews Genetics*, *8*, 299–309.

Burgess, D. J. (2015). Somatic mutations linked to future disease risk. *Nature Reviews Genetics*, *16*, 69.

Cawthon, R. M. (2002). Telomere measurement by quantitative PCR. *Nucleic Acids Research*, *30*, 47e.

Chen, J., Guo, L., Zhang, L., Wu, H., Yang, J., Liu, H., Wang, X., Hu, X., Gu, T., Zhou, Z., Liu, J., Liu, J., Wu, H., Mao, S. Q., Mo, K., Li, Y., Lai, K., Qi, J., Yao, H., ... Pei, D. (2013). Vitamin C modulates TET1 function during somatic cell reprogramming. *Nature Genetics*, *45*, 1504–1509.

Egerman, M. A., Cadena, S. M., Gilbert, J. A., Meyer, A., Nelson, H. N., Swalley, S. E., Mallozzi, C., Jacobi, C., Jennings, L. L., Clay, I., Laurent, G., Ma, S., Brachat, S., Lach-Trifilieff, E., Shavlakadze, T., Trendelenburg, A. U., Brack, A. S., & Glass, D. J. (2015). GDF11 increases with age and inhibits skeletal muscle regeneration. *Cell Metabolism*, *22*, 164–174.

Estes, B. T., Diekman, B. O., Gimble, J. M., & Guilak, F. (2010). Isolation of adipose-derived stem cells and their induction to a chondrogenic phenotype. *Nature Protocols*, *5*, 1294–1311.

Faubert, B., Vincent, E. E., Griss, T., Samborska, B., Izreig, S., Svensson, R. U., Mamer, O. A., Avizonis, D., Shackelford, D. B., Shaw, R. J., & Jones, R. G. (2014). Loss of the tumor suppressor LKB1 promotes metabolic reprogramming of cancer cells via HIF-1α. *Proceedings of the National Academy of Sciences*, *111*, 2554–2559.

Gontier, G., Iyer, M., Shea, J. M., Bieri, G., Wheatley, E. G., Ramalho-Santos, M., & Villeda, S. A. (2018). Tet2 rescues age-related regenerative decline and enhances cognitive function in the adult mouse brain. *Cell Reports*, *22*, 1974–1981.

Hannum, G., Guinney, J., Zhao, L., Zhang, L., Hughes, G., Sadda, S., Klotzle, B., Bibikova, M., Fan, J. B., Gao, Y., Deconde, R., Chen, M., Rajapakse, I., Friend, S., Ideker, T., & Zhang, K. (2013). Genome-wide methylation profiles reveal quantitative views of human aging rates. *Molecular Cell*, *49*, 359–367.

Katsimpardi, L., Litterman, N. K., Schein, P. A., Miller, C. M., Loffredo, F. S., Wojtkiewicz, G. R., Chen, J. W., Lee, R. T., Wagers, A. J., & Rubin, L. L. (2014). Vascular and neurogenic rejuvenation of the aging mouse brain by young systemic factors. *Science*, *344*, 630–634.

Li, L. C., & Dahiya, R. (2002). MethPrimer: Designing primers for methylation PCRs. *Bioinformatics*, *18*, 1427–1431.

Li, X., Yao, B., Chen, L., Kang, Y., Li, Y., Cheng, Y., Li, L., Lin, L., Wang, Z., Wang, M., Pan, F., Dai, Q., Zhang, W., Wu, H., Shu, Q., Qin, Z., He, C., Xu, M., & Jin, P. (2017). Ten-eleven translocation 2 interacts with forkhead box O3 and regulates adult neurogenesis. *Nature Communications*, *8*, 15903.

Liu, H., Zhu, X., Gu, Q., Wang, H., Liu, X., Zhao, E., Liu, X., Shen, J., Qin, B., Zhang, H., Gao, J., Zhang K., Quan W., Ruan, Q. Fu, L., Lin, Q., Li, D., Liu, J., Ge, W., Shen, H., Yu, Z., Sun, Y. E., (2020). GDF11 Rejuvenates Neural Stem Cells Via Smad2/3-PI3K-AKT-mTOR and Reverses Aged-Dependent Cognitive Decline. SSRN. or https://doi.org/10.2139/ssrn.3552151; https://ssrn.com/abstract=3552151

Liu, M. Y., DeNizio, J. E., & Kohli, R. M. (2016). Quantification of oxidized 5-methylcytosine bases and TET enzyme activity. *Methods in Enzymology*, *573*, 365–385.

Loffredo, F. S., Steinhauser, M. L., Jay, S. M., Gannon, J., Pancoast, J. R., Yalamanchi, P., Sinha, M., Dall'Osso, C., Khong, D., Shadrach, J. L., Miller, C. M., Singer, B. S., Stewart, A., Psychogios, N., Gerszten, R. E., Hartigan, A. J., Kim, M. J., Serwold, T., Wagers, A. J., & Lee, R. T. (2013). Growth differentiation factor 11 is a circulating factor that reverses age-related cardiac hypertrophy. *Cell*, *153*, 828–839.

Lyu, G., Guan, Y., Zhang, C., Zong, L., Sun, L., Huang, X., Huang, L., Zhang, L., Tian, X. L., Zhou, Z., & Tao, W. (2018). TGF-β signaling alters H4K20me3 status via miR-29 and contributes to cellular senescence and cardiac aging. *Nature Communications*, *9*, 2560.

Nadarajah, N., Meggendorfer, M., Kern, W., Haferlach, C., & Haferlach, T. (2015). Significance assessment of mutations in MDS patients using publicly available databases: A study with 944 samples and 6 most significantly mutated genes. *Blood*, *126*(23), 2849.

Njajou, O. T., Hsueh, W. C., Blackburn, E. H., Newman, A. B., Wu, S. H., Li, R., Simonsick, E. M., Harris, T. M., Cummings, S. R., & Cawthon, R. M. (2009). Association between telomere length, specific causes of death, and years of healthy life in health, aging, and body composition, a population-based cohort study. *The Journals of Gerontology: Series A*, *64*, 860–864.

Olson, K. A., Beatty, A. L., Heidecker, B., Regan, M. C., Brody, E. N., Foreman, T., Kato, S., Mehler, R. E., Singer, B. S., Hveem, K., Dalen, H., Sterling, D. G., Lawn, R. M., Schiller, N. B., Williams, S. A., Whooley, M. A., & Ganz, P. (2015). Association of growth differentiation factor 11/8, putative anti-ageing factor, with cardiovascular outcomes and overall mortality in humans: Analysis of the heart and soul and HUNT3 cohorts. *European Heart Journal*, *36*, 3426–3434.

Poggioli, T., Vujic, A., Yang, P., Macias-Trevino, C., Uygur, A., Loffredo, F. S., Pancoast, J. R., Cho, M., Goldstein, J., Tandias, R. M., Gonzalez, E., Walker, R. G., Thompson, T. B., Wagers, A. J., Fong, Y. W., & Lee, R. T. (2016). Circulating growth differentiation factor 11/8 levels decline with age. *Circulation Research*, *118*, 29–37.

Siddiqui, M. S., François, M., Fenech, M. F., & Leifert, W. R. (2015). Persistent γH2AX: A promising molecular marker of DNA damage and aging. *Mutation Research/Reviews in Mutation Research*, *766*, 1–19.

Sinha, M., Jang, Y. C., Oh, J., Khong, D., Wu, E. Y., Manohar, R., Miller, C., Regalado, S. G., Loffredo, F. S., Pancoast, J. R., Hirshman, M. F., Lebowitz, J., Shadrach, J. L., Cerletti, M., Kim, M. J., Serwold, T., Goodyear, L. J., Rosner, B., Lee, R. T., & Wagers, A. J. (2014). Restoring systemic GDF11 levels reverses age-related dysfunction in mouse skeletal muscle. *Science*, *344*, 649–652.

Smith, S. C., Zhang, X., Zhang, X., Gross, P., Starosta, T., Mohsin, S., Franti, M., Gupta, P., Hayes, D., Myzithras, M., Kahn, J., Tanner, J., Weldon, S. M., Khalil, A., Guo, X., Sabri, A., Chen, X., MacDonnell, S., & Houser, S. R. (2015). GDF11 does not rescue aging-related pathological hypertrophy. *Circulation Research*, *117*, 926–932.

Unnikrishnan, A., Freeman, W. M., Jackson, J., Wren, J. D., Porter, H., & Richardson, A. (2019). The role of DNA methylation in epigenetics of aging. *Pharmacology & Therapeutics*, *195*, 172–185.

Vincent, E. E., Coelho, P. P., Blagih, J., Griss, T., Viollet, B., & Jones, R. G. (2015). Differential effects of AMPK agonists on cell growth and metabolism. *Oncogene*, *34*, 3627–3639.

Walker, R. G., Czepnik, M., Goebel, E. J., McCoy, J. C., Vujic, A., Cho, M., Oh, J., Aykul, S., Walton, K. L., Schang, G., Bernard, D. J., Hinck, A. P., Harrison, C. A., Martinez-Hackert, E., Wagers, A. J., Lee, R. T., & Thompson, T. B. (2017). Structural basis for potency differences between GDF8 and GDF11. *BMC Biology*, *15*, 19.

Wu, D., Hu, D., Chen, H., Shi, G., Fetahu, I. S., Wu, F., Rabidou, K., Fang, R., Tan, L., Xu, S., Liu, H., Argueta, C., Zhang, L., Mao, F., Yan, G., Chen, J., Dong, Z., Lv, R., Xu, Y., ... Shi, Y. G. (2018). Glucose-regulated phosphorylation of TET2 by AMPK reveals a pathway linking diabetes to cancer. *Nature*, *559*, 637–641.

Wu, X., & Zhang, Y. (2017). TET-mediated active DNA demethylation: Mechanism, function and beyond. *Nature Reviews Genetics*, *18*, 517–534.

Young, J. I., Züchner, S., & Wang, G. (2015). Regulation of the epigenome by vitamin C. *Annual Review of Nutrition*, *35*, 545–564.

SUPPORTING INFORMATION

Additional supporting information can be found online in the Supporting Information section at the end of this article.

How to cite this article: Gao, J., Wang, H., Shen, J., Liu, X., Zhu, X., Huang, C., Li, G., Sun, Y., Liu, Z., Sun, Y. E., & Liu, H. (2023). Mutual regulation between GDF11 and TET2 prevents senescence of mesenchymal stem cells. *Journal of Cellular Physiology*, 1–14. https://doi.org/10.1002/jcp.31132